19th Australasian Tunnelling Conference – Acosta-Martínez, Stewart and Hudson-Smith (Eds.)

Selection of different arch shapes rock mass opening for underground space development – Considering rock support pressure requirements and spatial utilisation efficiency

Keith W.K. Kong
Sener Australia (formerly Tactix-Sener Group), Melbourne, Victoria, Australia

Jurij Karlovsek
School of Civil Engineering, The University of Queensland, St. Lucia, Queensland

ABSTRACT: A novel investigation has demonstrated that varying rock support pressures are required to maintain stable openings in rock masses, depending on the arch shape, specifically the roof arch rise-to-span ratio ranging from 0.1 to 0.4. Validated results indicate that optimised Q-system support pressures can be applied effectively across different arch geometries using rock reinforcement techniques. Notably, high-rise arch openings require approximately 19% less support pressure than low-rise configurations. These findings offer valuable insights for designing efficient and stable underground openings across diverse rock mass conditions. To gain deeper insight into the cost-benefit differences among various arch-shaped openings using rock reinforcement techniques, case studies were conducted comparing the number of rockbolts required and the total excavation volume generated. The results offer valuable indicators for underground space planners and constructors in selecting optimal opening geometries and support systems. This comparative analysis supports informed decision-making by balancing structural efficiency, sustainability, and economic viability in underground development projects.

1 INTRODUCTION

Underground rock openings are typically designed with arch-shaped roofs. However, limited research has explored how different arch geometries influence the engineering behavior of rock masses stabilised with reinforcement techniques. Kong et al. (2024) investigated this by constructing various arch-shaped openings under identical ground conditions and *in-situ* stress fields. Their findings revealed that high-rise arches exhibited less deformation than low-rise arches, a result that aligns with structural arch theory.

In terms of structural arch model, the arch distributes uniformly applied loads primarily through compression, generating horizontal thrust at its supports. Mikhelson (2004) emphasised that even under purely vertical loads, arches develop horizontal reactions, termed "thrust", denoted as $H_A = H_B$, as illustrated in Figure 1. As the arch rise decreases, the outward thrust increases, necessitating internal ties or external bracing at the arch abutments to maintain stability. This behavior implies that, for a constant span and vertical load, increasing the arch rise reduces deflection and horizontal thrust. Conversely, a low-rise arch under the same conditions demands greater horizontal reaction forces at the supports. Thus, high-rise arches give an enhancement of structural efficiency, offering a more stable configuration for underground openings.

The load-carrying capacity of structural arches can be applied to underground rock openings of varying arch geometries (Kong et al., 2024). Traditionally, the design of such openings has relied on empirical methods (e.g., Terzaghi, 1946; Unal, 1983; Goel & Jethwa, 1991; Barton et al., 1974; Osgoui & Ünal, 2009) or numerical simulations to estimate support pressures, particularly at the crown. However, most empirical approaches do not account for variations in roof shape. While several studies have examined different opening geometries, such as rectangular (Abdellah et al., 2018; Park et al., 2019), circular (Abdellah et al., 2018; Taghizadeh et al., 2020; Mazraehli & Zare,

2022; Varma et al., 2022), elliptical (Shiau et al., 2022; Taghizadeh et al., 2020; Wang et al., 2023), and horseshoe-shaped (Abdellah et al., 2018; Jia & Tang, 2008; Park et al., 2019), these analyses typically assume continuum media or infinite jointed rock masses. Critically, few studies have focused on how different arch shapes influence rock loading across varied rock mass conditions.

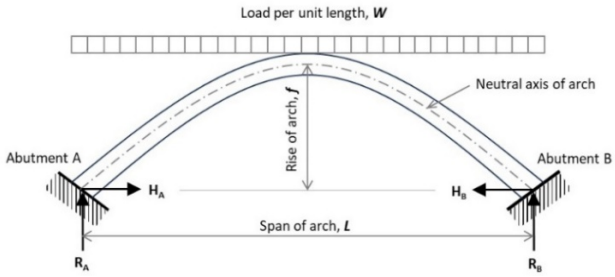

Where:

$H_A = H_B = W \cdot L^2 / 8f$, is horizontal reaction load at bearing point of the arch.

$R_A = R_B = W \cdot L / 2$, is vertical reaction load at bearing point of the arch.

Figure 1. Simple arch beam model and equations.

Kong et al. (2025) conducted a parametric desktop study to explore the maximum stable span of arch-shaped openings across a range of rock mass conditions. Their findings indicate that openings with rise-to-span ratios between 0.1 and 0.4, when using rock reinforcement technique, exhibit structural behaviors analogous to classical arches. The study demonstrated that different arch shapes, even under identical rock mass conditions, result in varying maximum stable spans. Consequently, each arch shape supports different rock loads due to its unique span capacity.

Building on these findings, a follow-up study was conducted to quantify the load-bearing capacity of various arch shapes across different rock mass conditions. This research produced practical design charts that estimate support pressure reductions based on the Q-system (Barton et al. 1974). Four validation models were simulated to verify the results, confirming that the proposed reductions in support pressure for different arch geometries are feasible. A cost-benefit analysis was also performed for openings of equal span but differing arch shapes. The analysis offers valuable guidance for selecting optimal opening geometries and stabilisation strategies that meet functional, operational, sustainability, and spatial requirements in underground space development.

2 DETAILED INVESTIGATION

2.1 *Maximum span opening*

Kong et al. (2025) conducted a parametric study using finite element method (FEM) simulations to evaluate the maximum feasible span of rock-reinforced caverns under varying geological conditions. The study involved 180 models, incorporating three Geological Strength Index (Hoek 1994; Hoek et al. 1995; Hoek & Brown 1997; Hoek et al. 1998; Marinos & Hoek 2001; Hoek & Brown 2019) values (GSI of 35, 45, 55), three uniaxial compressive strengths (UCS of 35, 70, 100 MPa), four arch geometries (rise-to-span ratios of 0.1 to 0.4), and five *in-situ* stress ratios [3, 2, 1.5, 1.25, as $\boldsymbol{k} = 0.5 + (150 / \text{depth})$ corresponding to depths of 60–300 m, respectively]. Based on the simulation results, the authors derived an empirical equation (Equation 1) to estimate the maximum stable span for caverns constructed in these conditions.

$$span = \left(\frac{F_{arc} \cdot E_{rm} \cdot I}{P_{roof} \cdot e^{F_s \cdot k}}\right)^{\frac{1}{4}} \quad (1)$$

Where F_{arc} = Roof arch factor, refer to Table 1; F_s = Load-stress factor; refer to Table 2; E_{rm} = Rock mass deformation modulus in MPa; I = Moment of Inertia of the "effective bolt length", i.e., (Bolt length – Bolt spacing)^3 / 12; P_{roof} = Q support pressure (Barton et al. 1974) in MPa; and $\boldsymbol{k}$ = *In-situ* stress ratio, i.e., horizontal stress / vertical stress.

In the study by Kong et al. (2025), rock reinforcement techniques were evaluated without incorporating a shotcrete protection liner to isolate the effects of rock reinforcement alone. The authors noted that including a shotcrete liner would introduce structural beam effects, contributing additional support to the excavation. While the primary role of shotcrete is to retain small wedge

failures between rock bolts, its design principles are beyond the scope of this paper. The investigation focused solely on rock reinforcement performance.

Table 1. Proposed roof arch factor (F_{arc}) of different roof arch geometries for the Equation (1).

Rise-to-Span Ratio of Arch	Arch Factor, F_{arc}
0.1	19.68
0.2	34.69
0.3	41.33
0.4	43.05

Table 2. Proposed load-stress factor (F_s) for the Equation (1).

Rock mass of 35 ≤ GSI ≤ 45		Rock mass of GSI = 55	
In-situ Stress *k*-ratio (Depth)	F_s	*In-situ* Stress *k*-ratio (Depth)	F_s
1.0 (300 m)	$3711.9 \cdot E_{rm}^{-0.715}$	1.0 (300 m)	$1E7 \cdot E_{rm}^{-1.66}$
1.25 (200 m)	$790.38 \cdot E_{rm}^{-0.578}$	1.25 (200 m)	$148526 \cdot E_{rm}^{-1.24}$
1.5 (150 m)	$504.25 \cdot E_{rm}^{-0.559}$	1.5 (150 m)	$2255.5 \cdot E_{rm}^{-0.813}$
2.0 (100 m)	$208.36 \cdot E_{rm}^{-0.485}$	2.0 (100 m)	$-9E\text{-}5 \cdot E_{rm} + 1.9683$
3.0 (60 m)	$348.57 \cdot E_{rm}^{-0.584}$	3.0 (60 m)	$-0.0001 \cdot E_{rm} + 1.984$

As outlined in Eq. (1), two rock mass groups, GSI 35–45 and GSI 55, were analysed. Results showed that, under identical ground and *in-situ* stress field conditions, different roof arch shapes produced varying maximum stable spans. The probable maximum span increased exponentially with the rock mass deformation modulus. Openings in fair quality rock mass (GSI = 55) supported significantly larger spans than those in lower-quality strata (GSI 35–45), highlighting the influence of rock mass quality and arch geometry on excavation stability.

2.2 *Methodology of the current investigation*

In this study, rock support load is estimated as the product of Q-support pressure and the opening span. According to the structural arch model and Dinnik's (1946) critical load theory, an arch's load-carrying capacity is proportional to its span. Kong et al. (2025) demonstrated that, under identical rock mass conditions and *in-situ* stress fields, different roof arch geometries yield varying maximum stable spans. Among these, the high-rise arch (Arch 0.4, with a rise-to-span ratio of 0.4) achieved the largest stable span.

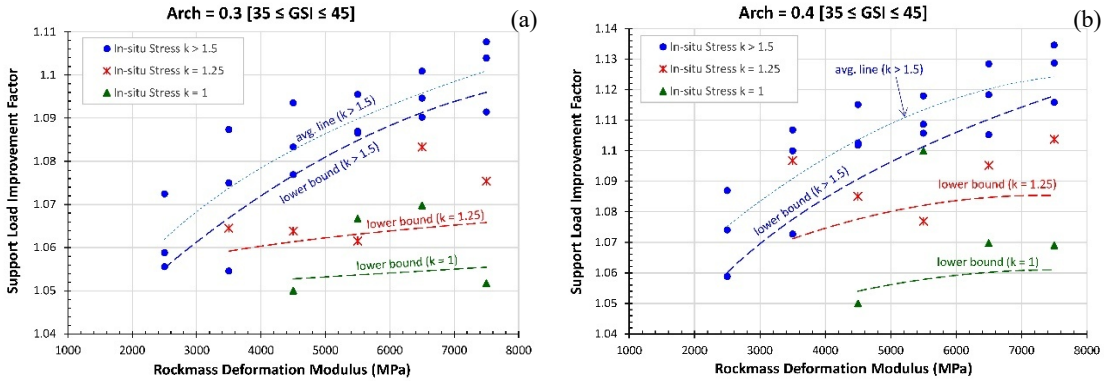

Figure 2. Recommended support load improvement factor for opening created in rock masses GSI 35–45 ground conditions. (a) Arch 0.3 opening. (b) Arch 0.4 opening.

To initiate the investigation into support pressure variations across arch shapes, a standard arch geometry with a rise equal to one-fifth of the span (Arch 0.2), as recommended by GEO (2018), was selected as the baseline for Q-support pressure. Using Eq. (1), the span differences between Arch 0.2 and Arch 0.3, and Arch 0.2 and 0.4 were expressed as fractions, representing relative load capacities. This ratio is termed the "Support Load Improvement Factor" for determining the Q-support pressure reduction. Results for Arches 0.3 and 0.4 are presented in Figure 2 (above)

and Figure 3 (below) for two rock mass groups of GSI 35–45 and GSI 55, corresponding approximately to Q-values of 0.2–1 and 4, respectively. It can be found that the Support Load Improvement Factor of Arch 0.1 is less than 1.0 because its opening span is smaller than Arch 0.2 opening (i.e. the base case) under the same rock mass conditions. These results are shown in Figure 4.

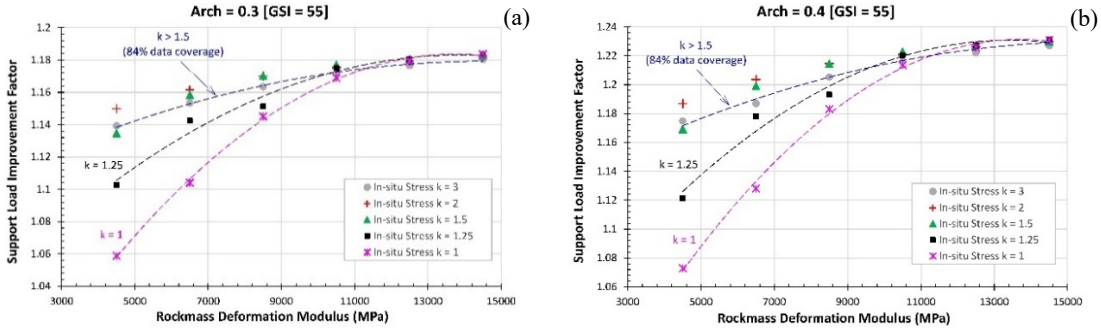

Figure 3. Recommended support load improvement factor for opening created in rock masses GSI = 55 ground conditions. (a) Arch 0.3 opening. (b) Arch 0.4 opening.

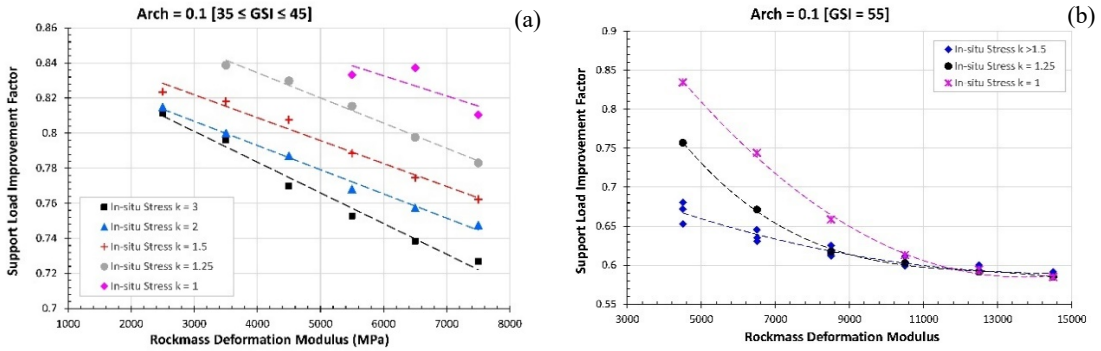

Figure 4. Support load improvement factor for Arch 0.1 opening created in a range of rock masses conditions. (a) opening created in rock masses GSI 35–45. (b) opening created in rock mass GSI = 55.

2.3 *Findings*

The investigation revealed that in poor rock mass conditions (GSI 35–45) with low rock mass deformation modulus, adopting alternative arch geometries can significantly reduce the required Q-support pressure. For example, using an Arch 0.3 shape instead of Arch 0.2 results in a support load reduction of at least 4.8%, calculated as '1 - 1/Support Load Improvement Factor'. For Arch 0.4, the reduction increases to approximately 5.7%. As the rock mass deformation modulus increases to 7.5 GPa, and under *in-situ* stress field conditions of $\boldsymbol{k} \geq 1.5$ (i.e., depths within 150 m), the required support pressure reductions rise to 9.5% and 12% for Arches 0.3 and 0.4, respectively. In media with a rock mass deformation modulus of 7.5 GPa and lower *in-situ* stress ($\boldsymbol{k}$ = 1.25 and 1.0, corresponding to depths of 200 m and 300 m), the reductions for Arch 0.3 range from 6.1% to 5.2%, and for Arch 0.4 from 7.8% to 5.7%.

In fair rock mass conditions (GSI = 55) with rock mass deformation modulus ≥ 4.5 GPa, more substantial reductions are observed. For Arch 0.3, support pressure savings range from 5.7% to 12.3% across *in-situ* stress fields from $\boldsymbol{k}$ = 1.0 to ≥ 1.5 respectively. Arch 0.4 offers even greater reductions, from 6.1% to 14.2% respectively. When the rock mass deformation modulus increases to 14.5 GPa, reductions converge to approximately 15.3% and 18.7% for Arches 0.3 and 0.4, respectively, regardless of *in-situ* stress conditions.

Conversely, an Arch 0.1 opening designed to match the maximum span of Arch 0.2 requires significantly more support due to its lower structural stiffness when using the same rockbolt pattern. However, if Arch 0.1 is constructed within its permissible span using reinforcement techniques, the Q-system (Barton et al. 1974) remains valid for estimating support pressure.

3 VALIDATION OF THE PROPOSED SUPPORT PRESSURE IMPROVEMENT

Original Arch 0.2 openings examined in the Kong et al. (2025) study were used as reference cases to validate the proposed Q-system support pressure reductions for Arches 0.3 and 0.4. The verification employed the RS2 (Rocscience, 2021), incorporating three main joint sets in a parallel deterministic pattern, consistent with Kong et al. (2025). Joint network configurations followed recommendations by Kong & Karlovsek (2024), yielding results closely aligned with field monitoring data. Opening stability was assessed using the Roof Sagging Ratio (RSR) criterion, where RSR > 0.50% indicates instability, as defined by Zhang & Mitri (2008), Abdellah (2015), and Abdellah et al. (2022). Input parameters for Models 1 and 2 are summarised in Table 3, with simulation outcomes illustrated in Figure 5.

Table 3. Parameters used for the original Arch 0.2 models from Kong et al. (2025).

Model	GSI	Rock Mass Deform. Mod.	Support Pressure	Bolt Spacing	Bolt Length	Depth of Opening	Opening Span
1	35	2.78 GPa	395 kPa	0.71 m	3.05 m	60 m	7 m
2	55	12.25 GPa	126 kPa	1.26 m	4.25	200 m	15 m

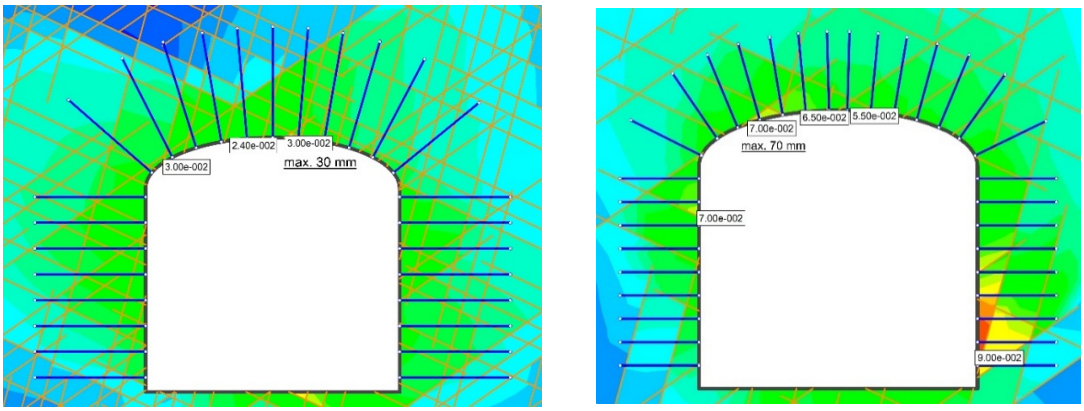

(a) Original Model 1 with Arch 0.2 (b) Original Model 2 with Arch 0.2

Figure 5. Simulation results for original Arch 0.2 models extracted from Kong et al. (2025).

In this validation study, the support load improvement factors for Arches 0.3 and 0.4 were derived from Figures 2 and 3, corresponding to basic Models 1 and 2, respectively. Verification results for these arches, developed under the conditions of Models 1 and 2, are summarised in Table 4 and presented in Figures 6 and 7.

Table 4. Comparison of validation results for Arch 0.3 and Arch 0.4 with original Arch 0.2 models.

Model	Original Arch 0.2				Arch 0.3				Arch 0.4			
	F	P_{roof}	D	RSR%	F	P_{roof}	D	RSR%	F	P_{roof}	D	RSR%
1	1	395	30	0.429	1.055	374.3	30	0.429	1.06	372.5	29	0.414
2	1	126	70	0.467	1.11	113.5	72	0.480	1.14	110.5	72	0.480

Notes: P_{roof} = Q-support pressure in kPa; D = Roof deformation at opening, in millimeters; F = Support Load Improvement Factor obtained from Figures 2 or 3; RSR% = Roof sagging ratio in percentage.

All results confirm the stability of the openings based on the RSR criterion, with less than 0.5% RSR detected. The difference in roof deformation (RSR%) between the baseline Arch 0.2 and Arches 0.3 and 0.4 remains below 3.5%. These findings validate the proposed Q-support pressure improvements for Arches 0.3 and 0.4 under the two rock mass conditions.

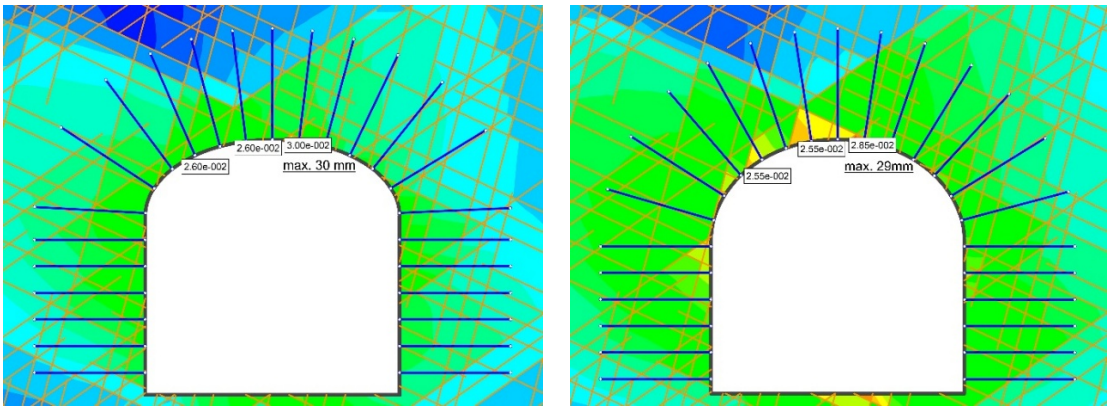

(a) Model 1 – Arch 0.3 (b) Model 1 – Arch 0.4

Figure 6. Validation models for Arches 0.3 and 0.4 created under identical conditions as Model 1.

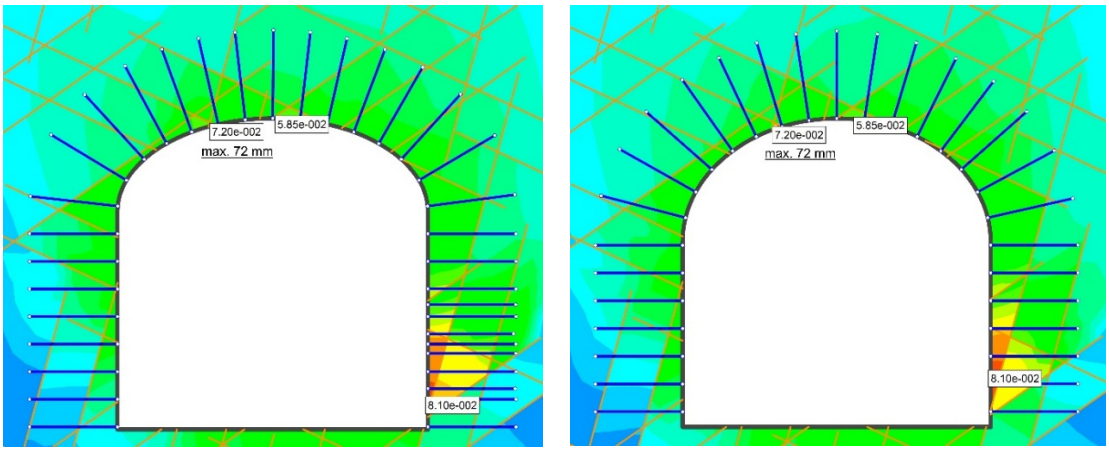

(a) Model 2 – Arch 0.3 (b) Model 2 – Arch 0.4

Figure 7. Validation models for Arches 0.3 and 0.4 created under identical conditions as Model 2.

4 COST BENEFIT COMPARISON AMONG DIFFERENT ARCH SHAPES OPENING

Several countries and regions including Australia (ATS 2024), Hong Kong (GEO 2018), Scandinavia (NGI 2015), Singapore (LTA 2019), the US (NHI 2009), and the UK (BTS & ICE 2004) recognise the Q-system for estimating support in arch-shaped rock mass openings. However, the current investigation reveals that different arch geometries require varying support pressures, even under identical ground conditions and spans. Notably, high-rise arches demand less support than the baseline Arch 0.2. Consequently, rockbolt spacing must be adjusted accordingly when using bolts of equal capacity. A cost-benefit comparison, considering rockbolt usage and excavation volume, was conducted for Arches 0.2, 0.3, and 0.4, using Models 1 and 2 as baselines. Detailed results are presented in Table 5.

Table 5 presents a comparative analysis of Models 1 and 2 under two scenarios. In Case 1, where full arch void utilisation is considered, such as in multi-lane road tunnels, the high-rise Arch 0.4 opening demonstrates advantages over the baseline Arch 0.2. It requires fewer rockbolts and results in reduced excavation volume due to lower support demands and wider bolt spacing. However, in Case 2, where wall height is the primary constraint, typical of underground powerhouses, the arch void offers limited spatial benefit. Here, high-rise arch openings may lead to increased rockbolt usage and greater excavation volume compared to Arch 0.2.

This cost-benefit comparison provides practical guidance for underground space designers, emphasizing the importance of aligning opening geometry with functional, spatial utilisation, and economic considerations.

Table 5. Constructability comparison among Arches 0.2, 0.3 and 0.4 openings.

Model 1 (GSI = 35) and Cavern Span = 7 m				Model 2 (GSI = 55) and Cavern Span = 15 m			
Aspect of Interest	Arch 0.2	Arch 0.3	Arch 0.4	Aspect of Interest	Arch 0.2	Arch 0.3	Arch 0.4
Arch Rise (m)	1.4	2.1	2.8	Arch Rise (m)	3	4.5	6
Arch Void Area, m²	7.7	11.6	15.4	Arch Void Area, m²	35.3	53.0	70.7
Arch Void % Diff	-	50.0	100.0	Arch Void % Diff	-	50.0	100.0
No. of Roof Bolts	11	13	13	No. of Roof Bolts	14	15	15
Bolts Spacing (m)	0.71	0.73	0.73	Bolts Spacing (m)	1.26	1.33	1.35
Case 1				Case 1			
Clear Opening Height*	7	7	7	Clear Opening Height*	15	15	15
No. of Wall Bolts	16	12	12	No. of Wall Bolts	18	16	14
Total of Bolts	27	25	25	Total of Bolts	32	31	29
X-sect. Area of Opening, m²	46.9	45.9	44.8	X-sect. Area of Opening, m²	215.3	210.5	205.7
X-sect. Area % Diff	-	-2.2	-4.5	X-sect. Area % Diff	-	-2.2	-4.5
Case 2				Case 2			
Fixed Wall Height#	5.6	5.6	5.6	Fixed Wall Height#	12	12	12
No. of Wall Bolts	16	16	16	No. of Wall Bolts	20	18	18
Total of Bolts	27	29	29	Total of Bolts	34	33	33
X-sect. Area of Opening, (m²)	46.9	50.8	54.6	X-sect. Area of Opening, (m²)	215.3	233.0	250.7
X-sect. Area % Diff	-	8.2	16.4	X-sect. Area % Diff	-	8.2	16.4

* denotes the overall height measured from invert to crown.
# denotes the height of the wall, measured from invert to bearing point of arch, i.e. the shoulder of the opening.

5 DISCUSSIONS AND CONCLUSIONS

The findings of this study demonstrate that arch-shaped openings require varying support pressures to maintain stability, even under identical ground conditions and spans. In better-quality rock masses with greater rock mass deformation modulus, high-rise arch openings demand up to 18.7% less support pressure than the baseline Arch 0.2 configuration that is estimated using the Q-system. This reduction translates to fewer rockbolts required for stabilisation due to decreased support loads and wider bolt spacing.

For openings exceeding the permissible span limits, a hybrid support system combining patterned rockbolts with concrete or shotcrete lining, is necessary to enhance lining stiffness and ensure structural stability.

Rock reinforcement remains a cost-effective and sustainable solution for underground development. This study presents a cost-benefit comparison across different arch geometries, offering valuable insights for designers and developers. The results support the selection of opening shapes that balance sustainability, functionality, spatial utilisation, and economic viability.

It is important to note that this study focused on two rock mass groups under specific conditions. Therefore, extrapolation beyond these parameters should be approached with caution. Further research is recommended to address these limitations and expand the applicability of the findings.

6 REFERENCES

ATS. 2024. *Tunnel Design Guideline*. Australian Tunnelling Society / Engineer Australia.

Abdellah, W.R.E. 2015. Numerical Modelling Stability Analyses of Haulage Drift in Deep Underground Mines. *J. Eng. Sci.*, 43(1), 71–81. https://doi.org/10.21608/jesaun.2015.115148

Abdellah, W.R., Ali, M.A. & Yang, H. 2018. Studying the effect of some parameters on the stability of shallow tunnels. *Journal of Sustainable Mining*, 17(1), 20–33.

Abdellah, W.R., Haridy, A.K.A., Mohamed, A.K., Kim, J. & Ali, M.A.M. 2022. Behaviour of Horseshoe-Shaped Tunnel Subjected to Different in Situ Stress Fields. *Appl. Sci.,* 2022, 12, 5399.

BTS & ICE. 2004. *Tunnel Lining Design Guide*. The British Tunnelling Society and The Institution of Civil Engineers. Thomas Telford, London, UK.
Barton N., Lien R. & Lunde J. 1974. Engineering Classification of Rock Masses for Design of Tunnel Support. *Rock Mech.,* 6, 189–236.
Dinnik, A.N. 1946. *The Stability of Arches*. Gostekhizdat, Moscow-Leningrad. (in Russian)
GEO. 2018. *Guide to Cavern Engineering*. 2nd Edition. Geotechnical Engineering Office, Civil Engineering Department, the Government of Hong Kong SAR.
Goel, R.K. & Jethwa, J.L. 1991. Prediction of support pressure using RMR classification. Proc. *Indian Getech. Conf.*, Surat, India, 203–205.
Hoek, E. 1994. Strength of Rock and Rock Masses. *ISRM News Journal*, 2(2), 4-16.
Hoek, E. & Brown, E.T. 1997. Practical estimates or rock mass strength. *Int. J. Rock Mech. & Mining Sci. & Geomechanics Abstr.*, 34(8), 1165–1186.
Hoek, E. & Brown, E.T. 1988. The Hoek-Brown failure criterion – a 1988 update. *Proceedings of the 15th Canadian Rock Mechanics Symposium*, 1988, 31–38.
Hoek, E. & Brown, E.T. 2019. The Hoek-Brown Failure Criterion and GSI - 2018 Edition. *J. Rock Mech. & Geotech. Eng.*, 11-3, 445–463. https://doi.org/10.1016/j.jrmge.2018.08.001
Hoek, E., Kaiser, P.K., & Bawden, W.F. 1995. *Support of Underground Excavations in Hard Rock*. Rotterdam, Balkema.
Kong, K.W.K. & Karlovsek, J. 2024. Recommended Rock Joints Setting in 2D FEM Simulations for Engineering Design of Excavations Created in Jointed Rock mass. Australian Journal of Multi-Disciplinary Engineering, 20(1), 88–106. https://doi.org/10.1080/14488388.2024.2328454
Kong, K., Rajabi, M. & Karlovsek, J. 2024. Natural Creation of Large Rock Cavern: Can We Construct Them? Jenolan Caves as a Case Study. Appl. Sci., 2024, 14, 10983.
Kong, W.K., Rajabi, M. & Karlovsek, J. 2025. How Wide Can a Rock-Reinforced Cavern Be Opened – a Parametric Desktop Investigation. Tunnelling and Underground Space Technology. Available at SSRN: http://dx.doi.org/10.2139/ssrn.5208677
Jia, P. & Tang, C.A. 2008. Numerical study on failure mechanism of tunnel in jointed rock mass. Tunnelling and Underground Space Technology, 23 (5), 500–507.
LTA. 2019. *Engineering Group – Civil Design Criteria for Road and Rail Transit Systems*, E/GD/09/106/A2. Land Transport Authority, Singapore Government.
Marinos, P. & Hoek, E. 2001. Estimating the Geotechnical Properties of Heterogeneous Rock Masses such as Flysch. *Bull. Engg. Geol. Env.*, 60, 85–92. https://doi.org/10.1007/s100640000090
Mazraehli, M. & Zare, S. 2022. Probabilistic Estimation of Rock Load Acting on Tunnels Considering Uncertainty in Peak and Post-peak Strength Parameters. *Geotech. Geol. Eng.*, 40, 2719–2736.
Mikhelson, L. 2004. *Structural Engineering Formulas*. Mcgraw-Hill.
NHI. 2009. *Technical Manual for Design and Construction of Road Tunnels – Civil Elements*. Publication No. FHWA-NHI-10-034. National Highway Institute, U.S. Department of Transportation, Federal Highway Administration, Washington, D.C. 20590.
NGI. 2015. Handbook – Using the Q-system : Rock Mass Classification and Support Design. Norwegian Geotechnical Institute, Oslo, Norway.
Osgoui, R.R. & Ünal, E. 2009. An empirical method for design of grouted bolts in rock tunnels based on the Geological Strength Index (GSI). *Engineering Geology*, 107, Issues 3-4, 154–166.
Park, D. & Michalowski, R.L. 2019. Roof stability in deep rock tunnels. *International Journal of Rock Mechanics & Mining Sciences*, 124, Article 104139.
Rocscience. 2021. *RS2 (formerly Phase² v9) Numercial Software Package*. Rocscience Inc. Toronto. www.rocscience.com
Shiau, J., Keawsawasvong, S. & Sorawit Seehavong, S. 2022. Stability of Unlined Elliptical Tunnels in Rock Masses. *Rock Mechanics and Rock Engineering*, 55, 7307–7330
Taghizadeh, H., Zare, S. & Mazraehli, M. 2020. Analysis of Rock Load for Tunnel Lining Design. *Geotech. Geol. Eng.*, 38, 2989–3005. https://doi.org/10.1007/s10706-020-01202-y
Terzaghi, K. 1946. Rock defects and loads on tunnel support. In R. V. Proctor and T. L. White (eds), *Introduction to Rock Tunnelling with Steel Supports. Section I*. Commercial Sheering & Stamping Co, Youngstown, Ohio, USA.
Ünal, E. 1983. *Design guidelines and roof control standards for coal mine roofs*. PhD thesis, Pennsylvania State University, University Park, 355p.
Varma, M., Maji, V.B. & Boominathan, A. 2022. Seismic Assessment of Shotcrete Support in Jointed Rock Tunnels. *International Journal of Geosynthetics and Ground Engineering*, 8, Article 51.
Wang, Y., Ling, K., Yang, Y., Zhang, Z., Xing S., He, M. & Liu, D. 2023. Experimental study on rockburst of surrounding rock in an elliptical tunnel with different axial ratios. *Tunnelling and Underground Space Technology*, 140, Article 105329. https://doi.org/10.1016/j.tust.2023.105329
Zhang, Y. And Mitri, H.S. 2008. Elastoplastic Stability Analysis of Mine Haulage Drift in the Vicinity of Mined Stopes. *Int. J. Rock Mech. & Min. Sci*., 45(4), 574–593.